NONCODING RNA

lncRNA *SLERT* controls phase separation of FC/DFCs to facilitate Pol I transcription

Man Wu[1]†, Guang Xu[1]†, Chong Han[1]†, Peng-Fei Luan[1], Yu-Hang Xing[1]‡, Fang Nan[2], Liang-Zhong Yang[1], Youkui Huang[1], Zheng-Hu Yang[1,3], Lin Shan[1], Li Yang[2,3], Jiaquan Liu[1]*, Ling-Ling Chen[1,3,4]*

RNA polymerase I (Pol I) transcription takes place at the border of the fibrillar center (FC) and the dense fibrillar component (DFC) in the nucleolus. Here, we report that individual spherical FC/DFC units are coated by the DEAD-box RNA helicase DDX21 in human cells. The long noncoding RNA (lncRNA) *SLERT* binds to DDX21 RecA domains to promote DDX21 to adopt a closed conformation at a substoichiometric ratio through a molecular chaperone–like mechanism resulting in the formation of hypomultimerized and loose DDX21 clusters that coat DFCs, which is required for proper FC/DFC liquidity and Pol I processivity. Our results suggest that *SLERT* is an RNA regulator that controls the biophysical properties of FC/DFCs and thus ribosomal RNA production.

L iquid-liquid phase separation is thought to drive the formation of nuclear condensates, including the nucleolus, which consists of subdomains containing distinct proteins and ribosomal RNAs (rRNAs) (1, 2). The complex organization is required for rDNA transcription coupled with pre-rRNA processing and ribosome production (2, 3). Each fibrillar center (FC) contains two to three transcriptionally active ribosomal DNAs (rDNAs) and is surrounded by mini liquid droplets of pre-rRNA processing factors that are further assembled into the dense fibrillar component (DFC) (Fig. 1A) (2). The rapid rRNA transcription occurs at the border of the FC and DFC, and the subsequent pre-rRNA processing takes place in the DFC (2, 3). Each nucleolus contains several dozen FC/DFC units that are embedded within one granular component (GC) region, which houses the later stage of pre-rRNA processing and ribosomal RNA ribonucleoprotein assembly (3).

Structured RNAs were recently found to play important roles in the assembly and function of phase-separated condensates (4–6). Whether any long noncoding RNA (lncRNA) is involved in the regulation of phase separation of the nucleolar components that gives rise to the layered composition of the nucleolus remains to be explored. *SLERT* is a box H/

ACA small nucleolar RNA (snoRNA)–ended lncRNA (Fig. 1, A and B). *SLERT* promotes RNA polymerase I (Pol I) transcription (fig. S1, A and B) by interacting with the DEAD-box RNA helicase DDX21 (7). We previously showed that upon *SLERT* binding, individual DDX21 molecules adopt a closed conformation (7). Loss of *SLERT* causes individual DDX21 molecules to switch to an open conformation and leads to the collapse of the DDX21-containing shell-like structure surrounding the FC, ultimately impairing Pol I transcription (7). In this study, we explored how *SLERT* controls DDX21 conformation and organization and consequently regulates the multilayered nucleolar architecture and Pol I–mediated transcription.

SLERT maintains appropriate size and mobility within FC/DFC units for Pol I transcription

We first confirmed the previous observation that *SLERT* is enriched in two to three spots in the DDX21 shell in each FC/DFC (7) (Fig. 1C). Consistent with (2), we found that DDX21 was largely localized outside of DFCs, whereas some DDX21 overlapped with FBL, which is a component of the DFC (Fig. 1D). DDX21 thus occupied a space in the shape of a shell, within which DDX21 was not uniform but appeared in patches (Fig. 1D).

CRISPR-Cas9–mediated *SLERT* knockout (KO) in human PA1 cells (fig. S1A) led to the reduced size of not only the DDX21 shell but also the entire FC/DFC unit (Fig. 1, E and F). Notably, the expression of examined FC/DFC proteins, including RPA194 and RPA49 (components of FC) (fig. S1C), and the number of FC/DFC units (fig. S1, D and E) in cells remained unaltered, suggesting that only the FC/DFC unit became more compact upon *SLERT* KO. A stochastic model of protein movement (8) predicts an increase in protein-protein interactions as the result of decreased spatial distribution. Indeed, we observed increased colocalization of RPA194 and FBL (Fig. 1G) and of FBL and DDX21 (fig. S1F) in PA1 cells.

Co-immunoprecipitation and pull-down assays confirmed their direct interactions (fig. S1, G to L). *SLERT* KO resulted in an increased interaction between them (fig. S1, M and N). mNeongreen-fused DDX21, FBL, RPA194, and RPA49 were less mobile in *SLERT* KO cells in a fluorescence recovery after photobleaching (FRAP) assay (Fig. 1H). Because the recruitment frequency of mammalian Pol I components is closely associated with Pol I processivity (9), the reduced RPA194 and RPA49 mobility suggests suppressed pre-rRNA transcription (fig. S1B). These results suggest that *SLERT* plays an essential role in maintaining the appropriate space and mobility within each FC/DFC unit for Pol I transcription.

DDX21 constrains FC/DFC size and liquidity

We next examined the assembly of DDX21 shell and DFC (Fig. 1D). Knockdown (KD) of FBL by short hairpin RNA in PA1 cells (fig. S2A) resulted in dispersed DDX21 distribution (Fig. 2A), whereas DDX21 KD (fig. S2A) led to larger FBL-labeled DFCs (Fig. 2B). Notably, FBL and DDX21 KD did not affect each other's expression (fig. S2A). These observations suggest that the formation of a DFC (2) is required for DDX21 assembly, but once formed, the DDX21 shell could constrain the size of the DFC as shown by FBL (Fig. 2B) and by another DFC marker, DKC1 (fig. S2B).

We next explored how the DDX21 shell restricted DFC size. FBL contains an N-terminal glycine and arginine-rich (GAR) domain with an intrinsically disordered region (IDR), and a C-terminal MD domain consisting of an RNA-binding domain and an alpha domain for methyltransferase activity (fig. S2C). DEAD-box RNA helicases can undergo phase separation in vitro (10). Prediction of the disorder tendency of DDX21 by IUPred2A (11) showed that DDX21 contains IDRs at each end (fig. S2C). Consistent with previous reports (1, 2), enhanced green fluorescent protein (EGFP)–FBL formed liquid-like droplets that had high mobility and were vulnerable to hexanediol (HEX) treatment and high salt in vitro (Fig. 2C and fig. S2, D to F). By contrast, N-terminal fusion of DDX21 with EGFP or mRuby3 (EGFP-DDX21 or mRuby3-DDX21) formed high-salt-sensitive, gel-like fibers that were resistant to HEX treatment (Fig. 2C and fig. S2, D to F).

Biochemical quantification revealed about 1×10^6 DDX21 and 0.6×10^6 FBL molecules per PA1 cell (fig. S3, A to C). Immunofluorescence intensity quantification showed that about 75% DDX21 and 80% FBL were in the nucleolus (fig. S3B). Given that each PA1 cell nucleus contains ~60 FC/DFC units (7), we estimated that each FC/DFC unit contained $~13 \times 10^3$ DDX21 and $~7.6 \times 10^3$ FBL molecules (fig. S3C). These calculations suggest that DDX21 and FBL are present at similar levels in each FC/DFC unit. In the following in vitro

[1]State Key Laboratory of Molecular Biology, Shanghai Key Laboratory of Molecular Andrology, CAS Center for Excellence in Molecular Cell Science, Shanghai Institute of Biochemistry and Cell Biology, University of Chinese Academy of Sciences, Chinese Academy of Sciences, 320 Yueyang Road, Shanghai, China. [2]CAS Key Laboratory of Computational Biology, Shanghai Institute of Nutrition and Health, Shanghai Institutes for Biological Sciences, University of Chinese Academy of Sciences, Chinese Academy of Sciences, Shanghai, China. [3]School of Life Science and Technology, ShanghaiTech University, Shanghai 201210, China. [4]School of Life Science, Hangzhou Institute for Advanced Study, University of Chinese Academy of Sciences, Hangzhou, China.
*Corresponding author. Email: liujiaquan@sibcb.ac.cn (J.L.); linglingchen@sibcb.ac.cn (L.-L.C.)
†These authors contributed equally to this work.
‡Present address: Department of Pathology, Massachusetts General Hospital and Harvard Medical School, Boston, MA 02114, USA.

Fig. 1. Loss of *SLERT* impairs the size and mobility of FC/DFC units. (**A**) A mammalian nucleolus comprises three subregions: FC, DFC, and GC. *SLERT* localizes primarily to the DFC. (**B**) A schematic of *SLERT* with box H/ACA snoRNAs (blue and yellow lines) at the termini. *SLERT* is located within the human *TBRG4* locus. (**C** and **D**) Colocalization of *SLERT*, DDX21, and FBL in the nucleolus by structured illumination microscopy (SIM) (C) and deconvolution imaging (D). (**E**) *SLERT* depletion leads to smaller ring structures of DDX21, FBL, and RPA194, as revealed by SIM (see fig. S1A). (**F**) *SLERT* KO reduces the size of DDX21, FBL, and RPA194 in PA1 cells. $n >$ 300 FC/DFC units. Data were analyzed by Imaris. Mann-Whitney test was used. Center line, median; upper and lower lines, upper and lower quartiles. (**G**) *SLERT* KO leads more Pol I to colocalize with FBL as shown by SIM on the left, with quantification shown on the right. $n >$ 40 cells. Mann-Whitney test was used. Means ± SD are shown. (**H**) Decreased mobility of FC/DFC components in *SLERT* KO PA1 cells by FRAP. Shaded regions indicate means ± SEM. Mann-Whitney test was used. $n >$ 6 cells. Data were analyzed by Fiji.
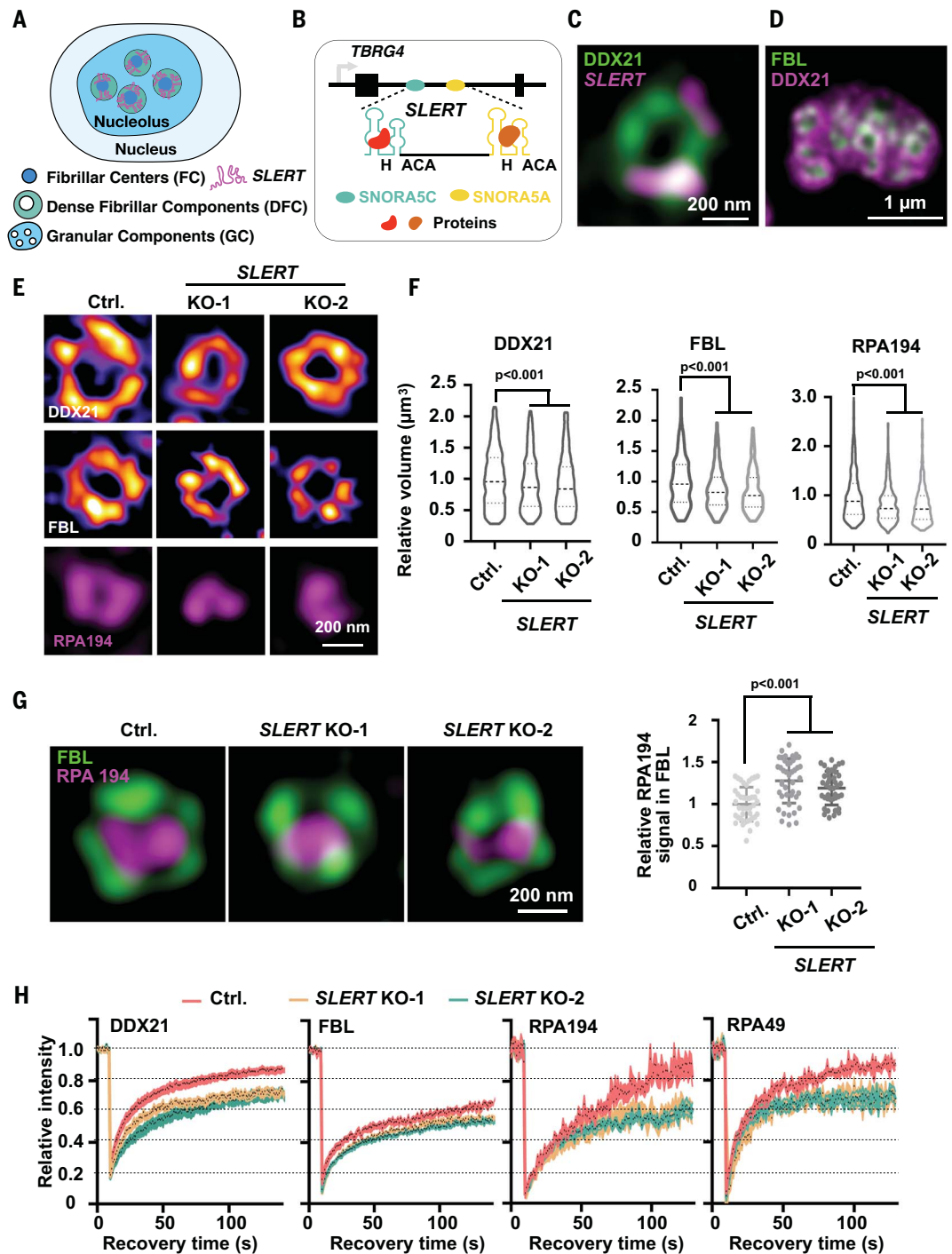
experiments, we considered them to be at a 1:1 stoichiometric ratio.

Consistent with the direct interaction of DDX21 with FBL (fig. S1, H and L), mixing EGFP-FBL and mRuby3-DDX21 at the same concentration (32 μM) led to completely colocalized gel-like fibers (fig. S4A). Reducing the ratio of mRuby3-DDX21 to EGFP-FBL resulted in the formation of EGFP-FBL droplets coated by mRuby3-DDX21 (fig. S4A), largely resembling their localization pattern in cells (Fig. 1D). Of note, FBL droplets formed in vitro

contain solely the FBL protein. This is different from the in vivo situation where each FC/DFC unit contains many other proteins. As controls, mRuby3-DDX21 protein alone formed gel-like fibers at most concentrations (1 to 32 μM) examined, except for the very low concentration of 0.5 μM (fig. S4A).

Notably, the size of EGFP-FBL droplets coated by mRuby3-DDX21 was negatively correlated with the concentration of mRuby3-DDX21 (Fig. 2D), consistent with the observation in cells, where DDX21 KD resulted in enlarged

FBL-labeled DFCs (Fig. 2B). Nonetheless, because we detected that DDX21 was highly mobile in normal cells (Fig. 1H), the formation of the static, gel-like DDX21 fibers in vitro (Fig. 2C and fig. S2E) suggests the existence of regulatory factor(s) in cells to promote DDX21 mobility in the nucleolus.

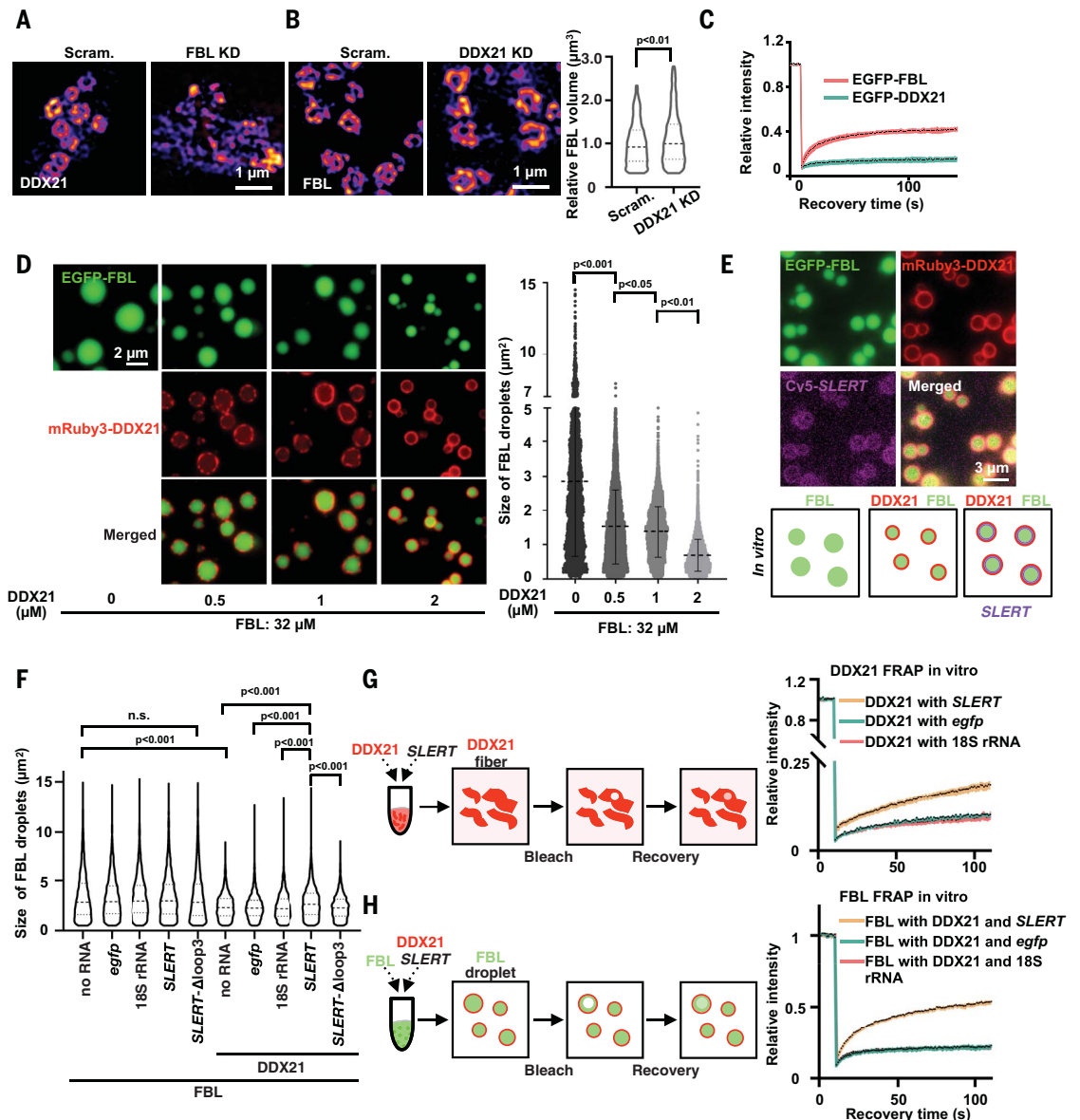### *SLERT* counteracts the effect of DDX21 on FC/DFC size and liquidity

Given the augmented DDX21-FBL interaction (fig. S1N) and the increased colocalization

Fig. 2. *SLERT* counteracts the effects of DDX21 on FC/DFC units. (**A**) DDX21 localization in scramble and FBL KD PA1 cells by SIM. (**B**) DDX21 KD leads to increased size of FBL rings. FBL in scramble and DDX21 KD PA1 cells by SIM is shown on the left; statistics of FBL rings in scramble and DDX21 KD cells is shown on the right. Mann-Whitney test was used. Center line, median; upper and lower lines, upper and lower quartiles. Data were analyzed by Imaris. *n* > 300 DFCs. (**C**) FRAP shows mobility of FBL and DDX21 in vitro. (**D**) DDX21 constrains the size of FBL droplets. mRuby3-DDX21 proteins coat EGFP-FBL droplets to form core-shell structures as shown by pseudocolor images on the left. Statistics of FBL droplets with different DDX21 concentrations are shown on the right. Data were analyzed by Imaris. *n* > 4000 FBL droplets. Mann-Whitney test was used. Center line, median; upper and lower lines, upper and lower quartiles. (**E**) FBL and DDX21 phase separation with *SLERT* as shown by pseudocolor images. The bottom graphics show an illustration of FBL, DDX21, and *SLERT* morphology

in vitro. (**F**) *SLERT* enlarges FBL droplets restricted by DDX21, as shown by phase separation assays with *SLERT* and control RNAs in FBL/RNA and FBL/DDX21/RNA condensates. Mann-Whitney test was used. Center line, median; upper and lower lines, upper and lower quartiles. Data were analyzed by Imaris. EGFP-FBL: 32 µM; mRuby3-DDX21: 1 µM; Cy5-RNA: 32 nM. *n* > 2500 FBL droplets. (**G**) FRAP shows the increased mobility of DDX21 with *SLERT* addition. DDX21: 25 µM; *SLERT/egfp*/18S rRNA: 0.25 µM. *n* > 10 DDX21 fibers. (**H**) FRAP shows the increased mobility of FBL with *SLERT* in FBL and DDX21 droplets. EGFP-FBL: 32 µM; mRuby3-DDX21: 1 µM; *SLERT/egfp*/18S rRNA: 0.32 µM. *n* > 10 FBL droplets.

between DDX21 and FBL-labeled DFCs (fig. S1F) upon *SLERT* KO, we hypothesized that *SLERT* could counteract the effect of DDX21 in constraining FC/DFC size. We observed a partial colocalization of Cy5-*SLERT* on mRuby3-DDX21-shell (Fig. 2E), and the addition of *SLERT*, but not of other control RNAs (fig. S4B), enlarged DDX21-coated FBL droplets (Fig. 2F and fig. S4C). Addition of *SLERT* also augmented the mobility of both DDX21 (Fig. 2G) and FBL within DDX21-coated droplets (Fig. 2H) and led to smaller DDX21 fibers, whereas addition of control RNAs did not show detectable changes (fig. S4D). In a sedimentation experiment (*12*), *SELRT* also notably attenuated

the formation of DDX21 fibers in a dosage-dependent manner (fig. S4E).

DDX21 proteins in their open conformation assemble into dense clusters that dampen FC/DFC liquidity and size

Multivalent interaction is often required for the assembly of phase-separated condensates (*13*). We next found that DDX21 formed intra- or intermolecular interactions by in vitro pull-down assays (fig. S5, A to D). Additional in vitro binding assays using a purified glutathione *S*-transferase (GST)–tagged C/N-domain of DDX21 (GST-DDX21-C/N) and His-tagged N/C-domain of DDX21 (His-mRuby3-DDX21-

N/C) (fig. S5C) revealed direct interactions of N/C, N/N, and C/C domains (fig. S5, E to G) with similar binding strengths (fig. S5H). These results suggest that the N and C termini of DDX21 mediate miscible intra- and inter-molecular interactions.

DDX21 switchable intra- and intermolecular interactions are associated with changeable protein conformations. We hypothesized that open and closed DDX21 conformations might lead to distinct biophysical properties of DDX21 clusters that surround DFCs (*14*). We mutated the conserved adenosine triphosphate (ATP)–binding amino acids GKT (Gly-Lys-Thr) to DAT (Asp-Ala-Thr) and the conserved ATP hydrolysis

Fig. 3. *SLERT* prompts the DDX21 closed conformation and loose state to ensure Pol I transcription.
(**A**) A schematic of DDX21$_{WT}$, its mutants, and the proposed closed or open conformation. (**B**) Intramolecular interaction of DDX21 in cells by FRET. Data were analyzed by Fiji. *n* > 15 cells. Mann-Whitney test was used. Means ± SD are shown. (**C**) Intermolecular interaction of DDX21 in cells by FRET (left). A schematic of the intermolecular interactions of DDX21$_{WT}$, DDX21$_{DAT}$, and DDX21$_{HGV}$ is shown on the right. Data were analyzed by Fiji. *n* > 15 cells. Mann-Whitney test was used. Means ± SD are shown. (**D**) DDX21$_{DAT}$ failed to rescue DFC in DDX21 KD PA1 cells. Statistics (left) and representative images by SIM (right) of FBL-marked DFCs in DDX21 KD cells with DDX21$_{WT}$, DDX21$_{DAT}$, or DDX21$_{HGV}$ overexpression are shown. n.s., not significant. *n* > 2000 FBL-marked DFCs. Mann-Whitney test was used. Center line, median; box limits, upper and lower quartiles; whiskers, maximum or minimum of the data. (**E**) DDX21$_{DAT}$ failed to rescue FC in DDX21 KD PA1 cells. Statistics (left) and representative images by SIM (right) of RPA194-marked FCs are shown. *n* > 2000 RPA194-marked FCs. Mann-Whitney

test was used. Center line, median; box limits, upper and lower quartiles; whiskers, maximum or minimum of the data. (**F**) The mobility of DDX21$_{WT}$ and mutants in PA1 cells. *n* > 10 cells. Means ± SEM are shown in the shaded regions. (**G**) The mobility of FBL, RPA194, and RPA49 in PA1 cells with DDX21$_{WT}$, DDX21$_{DAT}$, and DDX21$_{HGV}$ overexpression. *n* > 10 cells. Means ± SEM are shown in the shaded regions. (**H** and **I**) FRET of intramolecular (H) and intermolecular (I) interactions of DDX21$_{WT}$ in PA1 cells with or without *SLERT*. More than 15 cells are represented in each panel. Data were analyzed by Fiji. (**J**) A model shows how *SLERT* KO leads to conformational change of DDX21 to affect the FC/DFC.
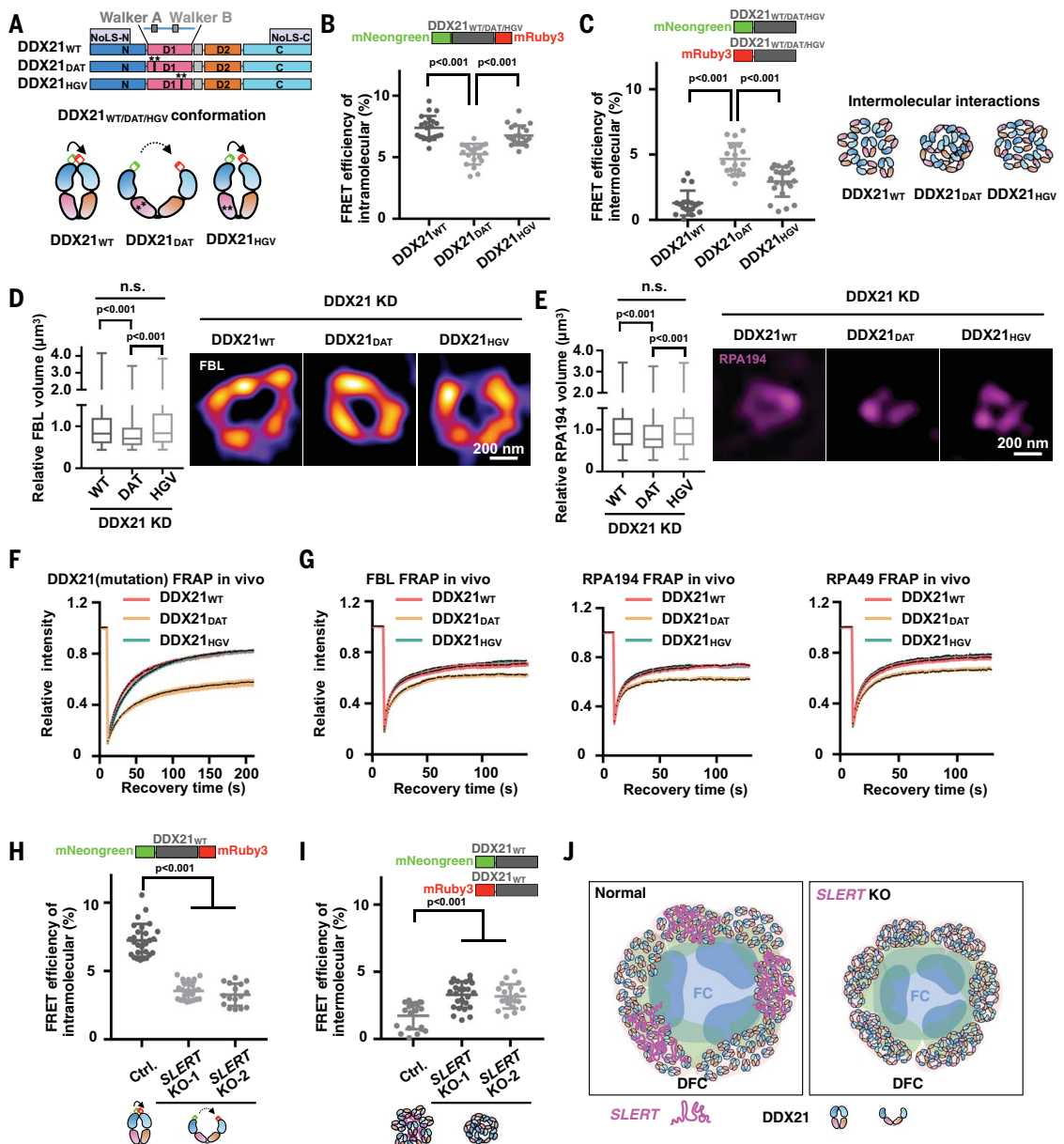
amino acids DEV (Asp-Glu-Val) to HGV (His-Gly-Val) (Fig. 3A) to abolish the catalytic activity (fig. S6, A to C). We tested intra- and intermolecular conformations of DDX21$_{DAT}$ and DDX21$_{HGV}$ using fluorescence resonance energy transfer (FRET). DDX21$_{DAT}$ displayed a dramatically reduced FRET signal (Fig. 3B), suggesting that loss of the ATP binding keeps DDX21$_{DAT}$ in an open conformation as reported (*15*, *16*) (Fig. 3A). DDX21$_{DAT}$ exhibited the highest intermolecular FRET efficiency in cells, compared with wild-type DDX21 (DDX21$_{WT}$) and DDX21$_{HGV}$ (Fig. 3C). Further, we con-

firmed enhanced polymer formation among purified DDX21$_{DAT}$ molecules compared with DDX21$_{WT}$ and DDX21$_{HGV}$ by native poly-acrylamide gel electrophoresis (PAGE) (fig. S6D). These results suggest that the open conformation of DDX21$_{DAT}$ results in augmented intermolecular interactions that cause the formation of dense DDX21$_{DAT}$ clusters, whereas DDX21$_{WT}$ and DDX21$_{HGV}$ proteins present a closed state, leading to loose DDX21 clusters (fig. S6D).

We next examined the impact of DDX21$_{WT}$, DDX21$_{DAT}$, and DDX21$_{HGV}$ on FC/DFC size and mobility in cells. DDX21$_{DAT}$ caused FCs

and DFCs to be of smaller size in DDX21 KD cells (Fig. 3, D and E) and to have a more reduced mobility as compared with DDX21$_{WT}$ and DDX21$_{HGV}$ (Fig. 3F), consistent with the compact status of DDX21$_{DAT}$ (Fig. 3C). DDX21$_{DAT}$ also limited the liquidity of DFCs and FCs (Fig. 3G and fig. S6E). Because DDX21$_{DAT}$ and DDX21$_{HGV}$ mutations both abolished the adenosine triphosphatase (ATPase) activity of DDX21 (fig. S6C), the reduced mobility and space in FC/DFC units observed in the presence of DDX21$_{DAT}$ are likely due to a DDX21$_{DAT}$ conformational change rather than their
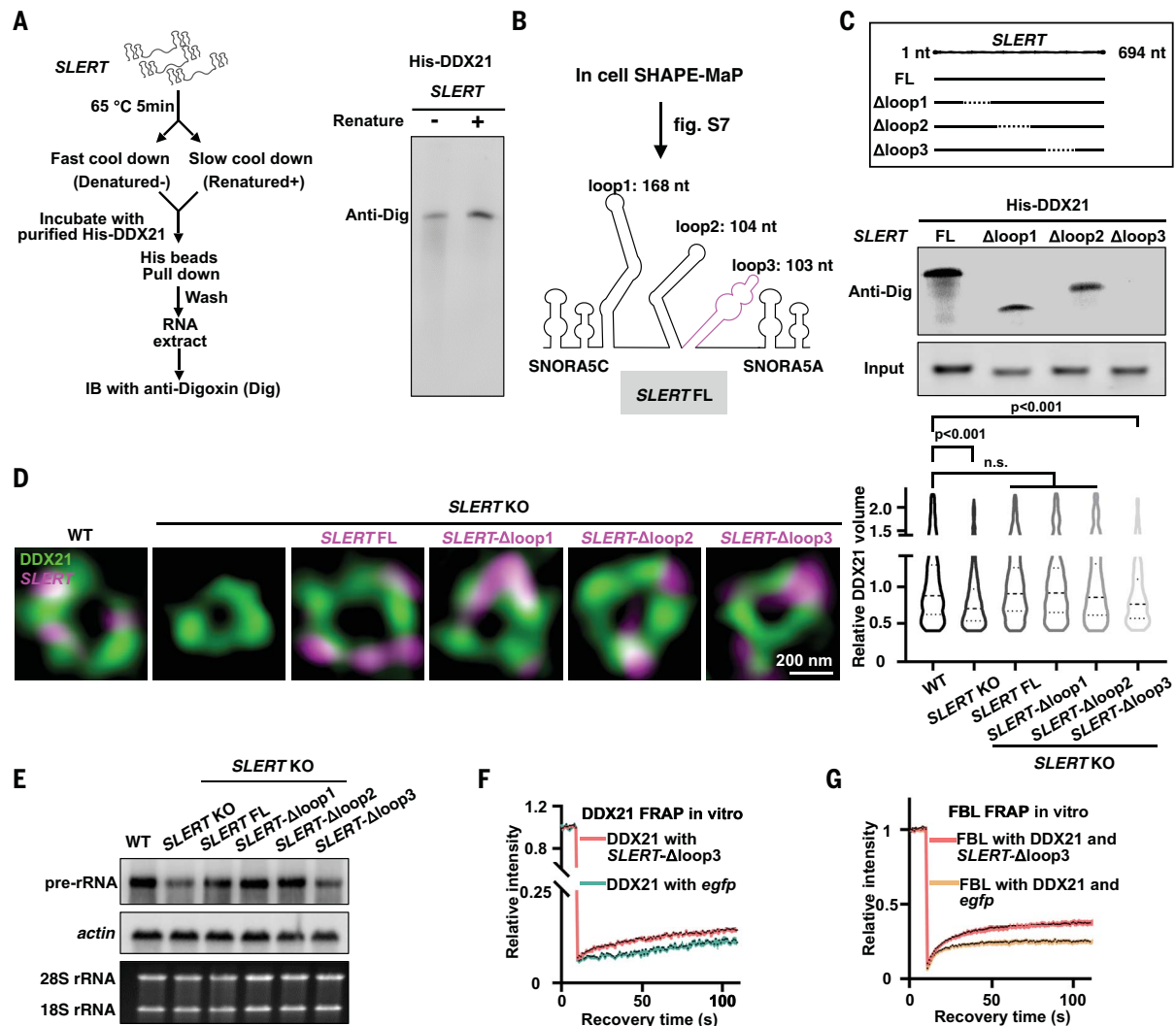
Fig. 4. An internal loop of *SLERT* interacts with DDX21 and is required for Pol I transcription. (**A**) In vitro binding assay of DDX21 and Dig-labeled *SLERT* shows that DDX21 tends to interact with structural *SLERT*. *SLERT* FL, full-length *SLERT;* IB, immunoblot. (**B**) An illustration shows *SLERT* structure by SHAPE-MaP (see fig. S7B). nt, nucleotides. (**C**) The loop 3 region of *SLERT* is required for *SLERT* and DDX21 interaction. *SLERT* FL and truncated fragments are is shown at the top; Northern blots of in vitro binding assay are shown at the bottom. (**D**) *SLERT*-Δloop3 could not rescue the size of DDX21 shells. Colocalization of *SLERT* FL and truncations with DDX21 in WT and *SLERT* KO PA1 cells by SIM is shown on the left; statistics of the size of DDX21 shells are shown on the right. *n* > 450 DDX21 shells. Mann-Whitney test was used. Center line, median; upper and lower lines, upper and lower quartiles. (**E**) *SLERT*-Δloop3 could not rescue pre-rRNA transcription in *SLERT* KO PA1 cells as shown by Northern blot. Total RNA collected from an equal number of cells across samples was loaded, and *actin* was a control RNA. (**F**) FRAP shows little increased mobility of DDX21 with *SLERT*-Δloop3 addition. DDX21: 25 μM; *egfp/SLERT*-Δloop3: 0.25 μM. *n* > 10 DDX21 fibers. (**G**) FRAP shows subtle increased mobility of FBL with addition of *SLERT*-Δloop3 in FBL and DDX21 droplets. FBL: 32 μM; DDX21: 1μM; *egfp/SLERT*-Δloop3: 0.32 μM. *n* > 10 FBL droplets.

impaired catalytic activity. Of note, ectopic expression of DDX21$_{DAT}$ drove the formation of a denser nucleolus (fig. S6, F and G).

SLERT promotes the formation of loose DDX21 patches in cells

SLERT loss (Fig. 1, F and H) and DDX21$_{DAT}$ expression (Fig. 3, D to G) both reduced the size and mobility of FC/DFC units. One speculation was that *SLERT* could modulate intra- and intermolecular interactions of DDX21. Indeed, a FRET assay revealed decreased intramolecular interactions (Fig. 3H) and increased intermolecular interactions of DDX21 (Fig. 3I)

upon *SLERT* KO. A native PAGE assay revealed augmented DDX21 multimerization, representing a dense state in *SLERT*-depleted cells (fig. S6H). Finally, because *SLERT* directly interacts with the D1 and D2 domains of DDX21 (*7*), *SLERT* might induce the DDX21 closed conformation by connecting these two domains. Indeed, an in vitro binding assay of truncated DDX21 showed increased association between N-D1 and D2-C domains upon *SLERT* addition at a ratio of 1:100 (RNA:protein) (fig. S6I). These results support the idea that *SLERT* regulates intra- and intermolecular interactions of DDX21 (Fig. 3J).

The positive effect of *SLERT* on Pol I transcription depends on a structured RNA domain

Next, we examined the key structural module(s) of *SLERT* in mediating its effect on controlling DDX21 conformational changes. First, DDX21 preferred to bind to structured but not denatured *SLERT* (Fig. 4A). Next, an optimized in vivo SHAPE-MaP (*17*) (fig. S7A) showed that *SLERT* possessed three internal loops apart from the two snoRNAs at its ends (Fig. 4B and fig. S7B). To identify the loop, if any, that specifically interacts with DDX21, we constructed *SLERT* truncated fragments (Fig. 4, B and C)

and found that the fragment without loop 3 (Δloop3) completely lost its binding to DDX21 in vitro (Fig. 4C). Mutation and replacement of *SLERT* loop 3 confirmed that this loop was essential for *SLERT*-DDX21 interaction (fig. S7C). Subsequently, *SLERT*-Δloop3 could not rescue the morphological changes of DDX21 shells or FC/DFC units in *SLERT* KO cells (Fig. 4D), even though *SLERT* mutants were still localized to DDX21 shells with the intact snoRNA ends (7) (Fig. 4D). Moreover, *SLERT*-Δloop3 failed to rescue the impaired Pol I transcription in *SLERT* KO cells (Fig. 4E), and unlike its full-length counterparts (Fig. 2, F to H), *SLERT*-Δloop3 was unable to enlarge DDX21-coated FBL droplets (Fig. 2F and fig. S4C) or increase DDX21 and FBL mobility (Fig. 4, F and G).

SLERT prevents DDX21 from hijacking rDNAs in FC/DFC units, resulting in enhanced Pol I transcription

An electrophoretic mobility shift assay (EMSA) confirmed the direct interaction between DDX21 and 28*S* rDNA (Fig. 5A) (7, 18). As controls, another *SLERT*-interacting, DEAD-box RNA helicase, DDX5 (7), barely bound 28*S* rDNA (fig. S8, A and B). These results suggest that the increased accessibility at the FC and DFC border upon *SLERT* depletion allows DDX21 clusters to directly bind and regulate transcribing rDNAs.

We used single-molecule total internal reflection fluorescent microscopy (smTIRF) to image direct interactions between rDNAs and DDX21 clusters in vitro (19) (Fig. 5B). A 14.3-kb DNA containing repeats of 28*S* rDNA sequences was constructed with one end linked to the quartz surface by means of a biotin-neutravidin interaction (Fig. 5B). Single DNA molecules were then stretched across a passivated flow cell surface by controlled laminar flow and visualized by Sytox Orange (fig. S8C left). Injection of DDX21-Cy5 resulted in DNA contraction and the colocalization of rDNA with DDX21 (Fig. 5C, fig. S8C, and movie S1). Kinetics of these progressions showed that DDX21-rDNA association and rDNA contraction occurred simultaneously (fig. S8D). DDX21-Cy5 formed miniclusters rather than monomers in solution (fig. S8E) at submicromolar concentrations (fig. S4A), where a single DDX21-Cy5 cluster is capable of binding two or more rDNAs (fig. S8F). DDX21 clusters could bind and wrap rDNAs at a nanomolar protein concentration (Fig. 5D), far below their cellular concentration (~1 μM) (20). As a control, DDX5 (fig. S8, A and B) was unable to wrap rDNA (fig. S8G), indicating that the rDNA occupation is specific for DDX21.

Injecting *SLERT* prevented DDX21 clusters from wrapping rDNA, even at an RNA:protein molar ratio of 1:100 (Fig. 5E and movie S2). EMSAs confirmed the specific role of *SLERT*

in preventing DDX21 clusters from binding rDNAs at substoichiometric levels (Fig. 5F), whereas 18*S* rRNA and *SLERT*-Δloop3 only mildly altered the rDNA-binding frequency of DDX21 (fig. S8H). Consistently, DDX21$_{DAT}$ that keeps DDX21 in an open conformation (Fig. 3, A to C) showed an augmented capability in wrapping rDNAs (fig. S8I). Distinct from *SLERT*, addition of rDNAs did not cause DDX21 conformational transition (fig. S8J). These observations together suggest that *SLERT* specifically induces the DDX21 closed conformation, which reluctantly binds rDNAs.

A single-molecule displacement assay that measures the mobility of DDX21 clusters further showed that *SLERT* can loosen the conformation of DDX21 clusters (Fig. 5G). DDX21-Cy5 (50 nM) on rDNA was slowly displaced by DDX21-Cy3 (50 nM) in solution, reflecting a relatively low mobility of DDX21 clusters (~7% replacement after 300 s) (Fig. 5G and fig. S9A). The presence of *SLERT* notably increased the DDX21 exchange rate (~53% replacement after 300 s; Fig. 5G and fig. S9, B and C), supporting the notion that *SLERT* relaxes DDX21 clusters to prevent rDNA hijacking (Fig. 5, E and F).

The key component of the Pol I complex, RPA49, binds to 28*S* rDNA (Fig. 5H and fig. S10A) (21). Addition of DDX21 reduced RPA49 binding on rDNA (Fig. 5H), and *SLERT* restored RPA49 occupancy on rDNA, as shown by smTIRF (Fig. 5I and fig. S10, B and C). These observations are in line with the reduced RPA49 occupancy on rDNA (fig. S10D) and increased colocalization between DDX21 and rDNAs upon *SLERT* KO in cells (fig. S10E). Of note, DDX21 localizes to FC/DFC units that harbor active rDNAs, but not to inactive rDNAs (fig. S10F), consistent with the FBL-dependent assembly of DDX21 patches (Fig. 2, A and B).

SLERT modulates DDX21 multimer-to-monomer transitions at substoichiometric ratios through a molecular chaperone–like mechanism

An improved RNA extraction method for nuclear RNAs (22) revealed around 800 copies of *SLERT* per cell (fig. S11, A to D). Given ~60 FC/DFC units in a single PA1 cell (7), each unit was estimated to contain 13 *SLERT* molecules (fig. S11E), 1000-fold less than DDX21 molecules (13×10^3 per unit; fig. S3). It is worthwhile to note that the local *SLERT*:DDX21 ratio within one rDNA unit should be higher than 1:1000 because *SLERT* is largely located adjacent to RPA194-labeled active rDNAs (Fig. 6, A and B) (2).

How does *SLERT* regulate DDX21 conformational change at a substoichiometric ratio? One hypothesis is that *SLERT* can act as an RNA chaperone. Several lines of evidence support this idea. The molecular ratio of *SLERT* and DDX21 within one cluster in solution is ~1:70 (fig. S12A). DDX21 underwent gradually reduced multimerization when incubated with

gradually increased levels of *SLERT* (Fig. 6, C and D). The change was observed even at a 1:1000 stoichiometric ratio of *SLERT* to DDX21 (Fig. 6C). Furthermore, when *SLERT* was continuously supplemented in a smTIRF system at a 1:100 ratio, it took ~2 min to execute one cycle of *SLERT* binding and DDX21 conformation alteration on rDNA (Fig. 6, E and F). Consistently, the multimer-to-monomer transition of DDX21 was observed at 2 min by incubating with a limited amount of *SLERT* (Fig. 6G), and this transition became dramatic with prolonged incubation times (Fig. 6, G and H), suggesting the capability of *SLERT* to continuously alter DDX21 conformation in the system, a key feature of a molecular chaperone. As controls, other RNAs did not induce a DDX21 conformational switch within the examined periods (fig. S12, B to D). Moreover, *SLERT* prefers to bind DDX21$_{DAT}$ (fig. S12E), raising the possibility that once *SLERT* induces a DDX21 to adopt the closed conformation, this DDX21 would be released, allowing the recruitment of another DDX21 with an open conformation to initiate another cycle of conformational transition (Fig. 6I). Consistently, even at a 1:1000 substoichiometric ratio of *SLERT* and DDX21, multimer-to-monomer transitions of DDX21 clusters were observed with prolonged incubation (fig. S12F).

Discussion

Our biochemical analyses revealed that *SLERT*, like protein chaperones, can continuously induce a DDX21 multimer-to-monomer switch in a time-dependent manner (Fig. 6, G to I; and fig. S12). How exactly *SLERT* works as a molecular chaperone and whether any other RNAs possess such chaperone-like capability warrants future investigation. Other functional lncRNAs, such as *Xist* (23), have also been shown to modulate their interacting proteins at a substoichiometric concentration without a known mechanism. Canonical chaperone proteins such as Hsp27 (24), HDJ1, and Hsp104 (25) act in substoichiometric ratios to chaperone FUS (1:50) or α-synuclein (1:200) within their phase separated droplets to prevent the transition into amyloid fibrils; whether RNA chaperones, like *SLERT*, act similarly as these protein chaperones warrants additional mechanistic studies.

Within FC/DFCs, *SLERT*-induced DDX21 hypomultimerization facilitates Pol I processivity and rDNA transcription through a dual effect. First, the loosened DDX21 clusters that coat DFCs in the presence of *SLERT* ensure the appropriate space and liquidity in FC/DFC condensates required for rDNA transcription to occur at the FC/DFC border (Fig. 1). This also provides an explanation for how *SLERT* loosens DDX21 rings (7). Second, *SLERT*-induced DDX21 hypomultimerization prevents DDX21 clusters from hijacking rapidly transcribing
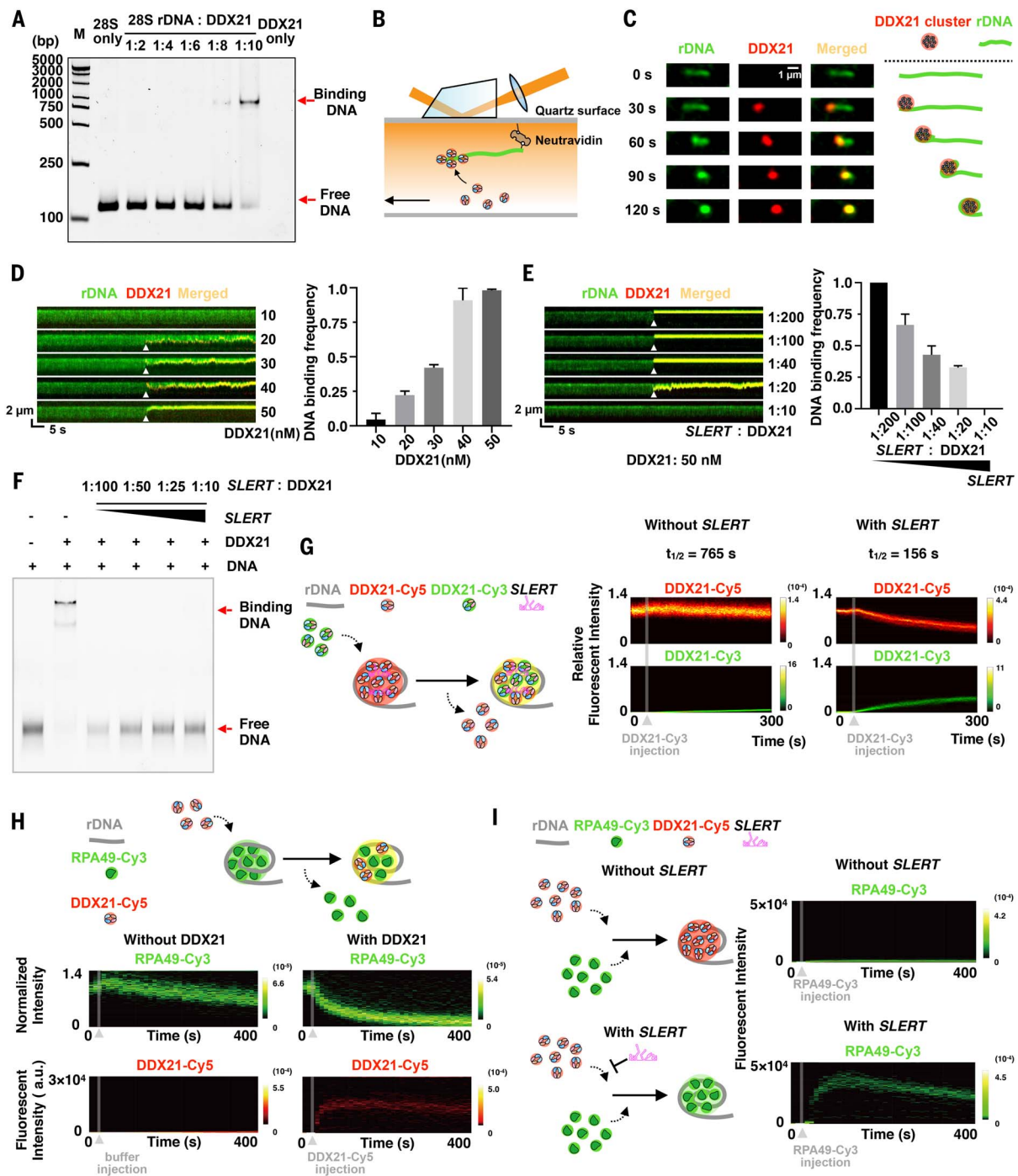
Fig. 5. *SLERT* increases DDX21 cluster mobility and prevents DDX21 from wrapping rDNA. (**A**) 28S rDNA fragment interacts with DDX21, as shown by EMSA. bp, base pairs. (**B**) A schematic of rDNA-DDX21 interactions by smTIRF. (**C**) DDX21 cluster (red) binds and wraps rDNA (green). (**D**) Representative kymographs showing rDNA binding with DDX21. Arrowheads indicate the association of DDX21 with rDNA. The rDNA binding frequency with DDX21 is shown. Error bars represent means ± SD. (**E**) *SLERT* prevents DDX21 clusters from wrapping rDNA shown by kymographs of rDNA binding under various *SLERT*:DDX21 substoichiometric ratios (left) and rDNA binding frequencies (right). Error bars represent means ± SD. (**F**) *SLERT* prevents DDX21 from binding rDNA, as shown by EMSA. (**G**) *SLERT* promotes replacement of DDX21 on rDNA. Normalized fluorescent density plots of DDX21 cluster as functions of time without *SLERT* (left, $n = 79$ molecules) and with *SLERT* (right, $n = 45$). The observed exchange half-life ($t_{1/2}$) is shown. Intensity bars indicate relative frequencies in density plots (low, black; high, yellow). (**H**) DDX21-Cy5 binding results in RPA49 dissociation from rDNA. Fluorescent density plots of RPA49 (green) and DDX21 (red) as functions of time. $n = 64$ (without DDX21) or 82 (with DDX21) molecules. (**I**) *SLERT* evicts DDX21-Cy5 from binding RPA49-rDNA. rDNAs were preincubated with DDX21-Cy5 (with or without *SLERT*), followed by RPA49-Cy3 injection. Fluorescent density plots of RPA49 as functions of time are shown. $n = 132$ (without *SLERT*) or 110 (with *SLERT*) molecules.
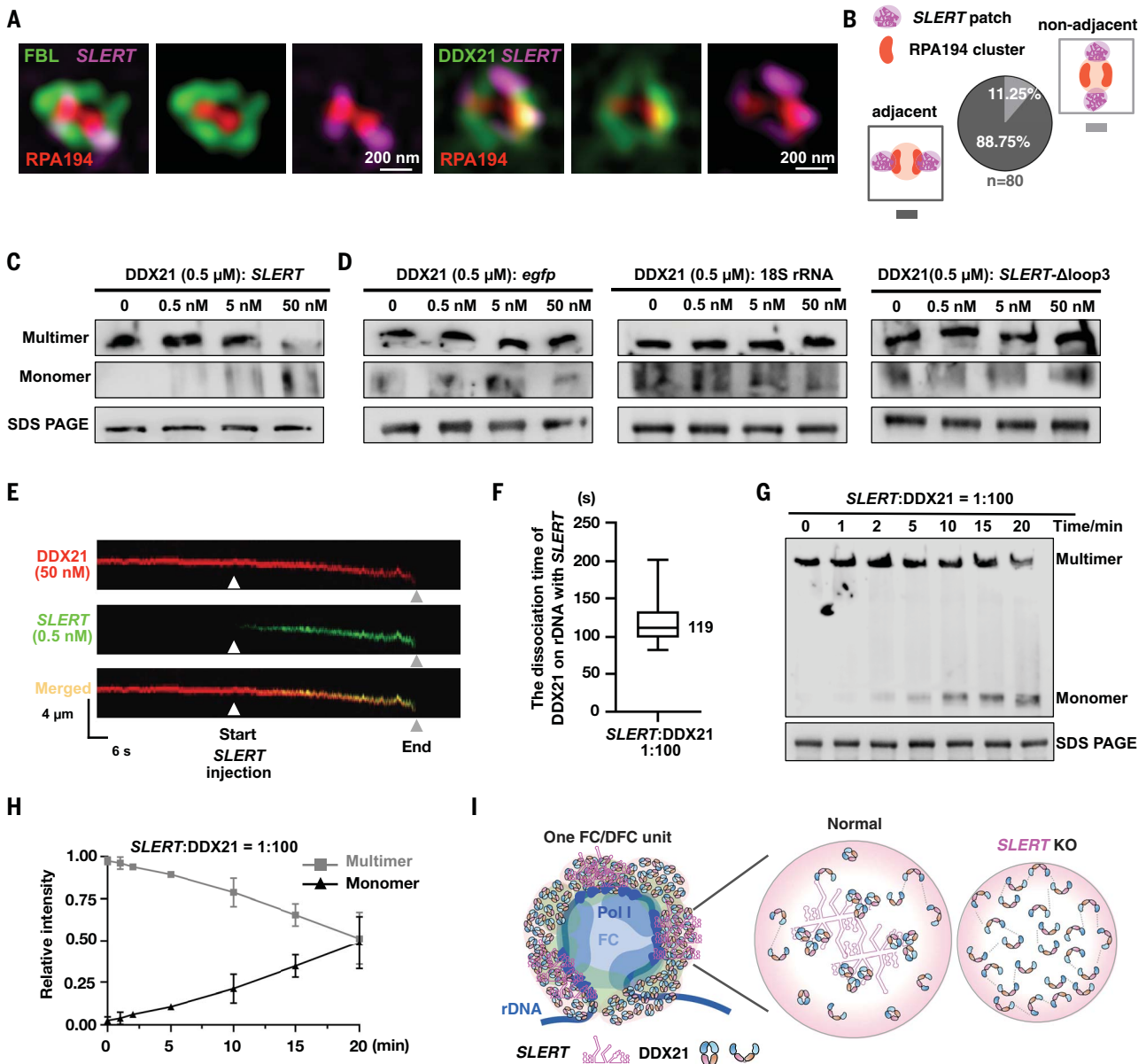
Fig. 6. *SLERT* chaperones DDX21 multimer-to-monomer transitions at a substoichiometric ratio. (**A**) Localization of FBL or DDX21 (green), RPA194 (red), and *SLERT* (purple) by SIM. (**B**) The schematic and statistics of the relation between RPA194 and *SLERT*. The two gray rectangles represent the two distribution patterns between RPA194 and *SLERT*. (**C**) *SLERT* decreases DDX21 multimerization, as shown by native Western blot of DDX21 incubated with *SLERT*. (**D**) *egfp*, 18*S* rRNA, and *SLERT*-Δloop3 have no detectable effect on DDX21 multimerization, as shown by native Western blot. (**E**) Representative kymographs showing that *SLERT* binds a DDX21 cluster and induces the dissociation of DDX21 from rDNA. DDX21-Cy5: 50 nM; *SLERT*-Cy3: 0.5 nM. (**F**) The mean dissociation time of

DDX21 clusters upon *SLERT* binding in Fig. 6E. The black line shows the mean, box ends show the quartiles (25 and 75%), and whiskers show the maximum or minimum of the data. (**G**) *SLERT* promotes DDX21 multimer-to-monomer transitions at a 1:100 ratio in a time-dependent manner. Native Western blot of DDX21 incubated with *SLERT* for different times is shown. (**H**) Statistics of the relative intensity of DDX21 multimers and monomers from Fig. 6G. Error bars represent means ± SD. (**I**) A proposed model of how *SLERT* promotes DDX21 multimer-to-monomer transitions within patches at a substoichiometric ratio in one FC/DFC unit by a chaperone-like mechanism. The dotted line represents the intermolecular interaction of DDX21.

rDNAs (Fig. 5 and figs. S8 to S10) required for protein homeostasis and cellular function. In this scenario, phase separation acts by providing proper space and mobility within FC/DFC units to achieve a rapid Pol I processivity (fig. S13). Of note, such a mechanism is different from phase separation that acts to locally concentrate transcriptional factors, transcrip-

tional coactivators, and RNA polymerase II (Pol II) components at Pol II–transcribed genes (*26–29*).

REFERENCES AND NOTES

1. M. Feric et al., Cell **165**, 1686–1697 (2016).
2. R. W. Yao et al., Mol. Cell **76**, 767–783.e11 (2019).
3. F. M. Boisvert, S. van Koningsbruggen, J. Navascués, A. I. Lamond, Nat. Rev. Mol. Cell Biol. **8**, 574–585 (2007).
4. T. Yamazaki et al., Mol. Cell **70**, 1038–1053.e7 (2018).
5. A. Jain, R. D. Vale, Nature **546**, 243–247 (2017).
6. E. M. Langdon et al., Science **360**, 922–927 (2018).
7. Y. H. Xing et al., Cell **169**, 664–678.e16 (2017).
8. R. D. Phair, T. Misteli, Nature **404**, 604–609 (2000).
9. M. Dundr et al., Science **298**, 1623–1626 (2002).
10. M. Hondele et al., Nature **573**, 144–148 (2019).
11. B. Mészáros, G. Erdos, Z. Dosztányi, Nucleic Acids Res. **46**, W329–W337 (2018).

12. A. Yamasaki et al., Mol. Cell **77**, 1163–1175.e9 (2020).
13. P. Li et al., Nature **483**, 336–340 (2012).
14. E. Jankowsky, Trends Biochem. Sci. **36**, 19–29 (2011).
15. R. Futamata et al., J. Biol. Chem. **295**, 5002–5011 (2020).
16. Z. Chen et al., Adv. Sci. **7**, 2000532 (2020).
17. R. C. Spitale et al., Nat. Chem. Biol. **9**, 18–20 (2013).
18. E. Calo et al., Nature **518**, 249–253 (2015).
19. J. Liu et al., Nature **539**, 583–587 (2016).
20. M. Y. Hein et al., Cell **163**, 712–723 (2015).
21. S. R. Geiger et al., Mol. Cell **39**, 583–594 (2010).
22. T. Chujo et al., EMBO J. **36**, 1447–1462 (2017).
23. Y. Markaki et al., bioRxiv 2020.11.22.393546 [Preprint] (2020); https://doi.org/10.1101/2020.11.22.393546.
24. Z. Liu et al., Nat. Struct. Mol. Biol. **27**, 363–372 (2020).
25. C. Jia et al., Front. Neurosci. **13**, 1124 (2019).
26. A. Boija et al., Cell **175**, 1842–1855.e16 (2018).
27. W. K. Cho et al., Science **361**, 412–415 (2018).
28. B. R. Sabari et al., Science **361**, eaar3958 (2018).
29. Y. E. Guo et al., Nature **572**, 543–548 (2019).

SUPPLEMENTARY MATERIALS

science.sciencemag.org/content/373/6554/547/suppl/DC1
Materials and Methods
Figs. S1 to S13
Table S1
References (30–40)
MDAR Reproducibility Checklist
Movies S1 and S2

View/request a protocol for this paper from Bio-protocol.

Science

lncRNA *SLERT* controls phase separation of FC/DFCs to facilitate Pol I transcription

Man Wu, Guang Xu, Chong Han, Peng-Fei Luan, Yu-Hang Xing, Fang Nan, Liang-Zhong Yang, Youkui Huang, Zheng-Hu Yang, Lin Shan, Li Yang, Jiaquan Liu and Ling-Ling Chen

Keeping the nucleolus a liquid condensate

The nucleolus is a multilayered, membraneless nuclear condensate in which DNA polymerase I (Pol I)–mediated ribosomal DNA (rDNA) transcription and pre-rRNA processing occur in fibrillar center and dense fibrillar component (FC/DFC) units. How the biophysical properties of the nucleolus are regulated has remained elusive. Wu *et al.* found that the RNA helicase DDX21 forms a shell coating each FC/DFC unit in the nucleolus (see the Perspective by Yamazaki and Hirose). The authors found that a long noncoding RNA called *SLERT* facilitates the transition from the open to the closed configuration of the helicase using a chaperonelike mechanism. DDX21 in the closed conformation forms loose clusters that confer the FC/DFC unit sufficient liquidity and space required for Pol I processivity. In addition, DDX21 within the loose clusters cannot approach and wrap rDNA, thus licensing rDNA for transcription.
Science, abf6582, this issue p. 547; see also abj8350, p. 486

ARTICLE TOOLS	http://science.sciencemag.org/content/373/6554/547
SUPPLEMENTARY MATERIALS	http://science.sciencemag.org/content/suppl/2021/07/28/373.6554.547.DC1
RELATED CONTENT	http://science.sciencemag.org/content/sci/373/6554/486.full
REFERENCES	This article cites 40 articles, 8 of which you can access for free http://science.sciencemag.org/content/373/6554/547#BIBL
PERMISSIONS	http://www.sciencemag.org/help/reprints-and-permissions

Use of this article is subject to the Terms of Service